NANO · MICRO small
www.small-journal.com

Atom Probe Tomography for 3D Structural and Chemical Analysis of Individual Proteins

*Gustav Sundell, Mats Hulander, Astrid Pihl, and Martin Andersson**

Determination of the 3D structure of proteins and other biomolecules is a major goal in structural biology, to provide insights to their biological function. Such structures are historically unveiled experimentally by X-ray crystallography or NMR spectroscopy, and in recent years using cryo-electron microscopy. Here, a method for structural analysis of individual proteins on the sub-nanometer scale using atom probe tomography is described. This technique offers a combination of high-resolution analysis of biomolecules in 3D, and the chemical sensitivity of mass spectrometry. As a model protein, the well-characterized antibody IgG is used. IgG is encapsulated in an amorphous solid silica matrix via a sol–gel process to provide the requisite support for atom probe analysis. The silica synthesis is tuned to resemble physiological conditions. The 3D reconstructions show good agreement with the protein databank IgG crystal structure. This suggests that the silica-embedding strategy can open the field of atom probe tomography to the analysis of biological molecules. In addition to high-resolution structural information, the technique may potentially provide chemical information on the atomic scale using isotopic labeling. It is envisaged that this method may constitute a useful complement to existing tools in structural biology, particularly for the examination of proteins with low propensity for crystallization.

A critical aspect of the field of structural biology is to characterize the structure of proteins in three dimensions. Traditionally, the functional structure of proteins has been determined using X-ray crystallography[1] or nuclear magnetic resonance (NMR).[2] In recent years, considerable progress has been made by the application of cryo-electron microscopy[3] to biological structures. In this study, we demonstrate a new method to study 3D structure and composition of proteins simultaneously. The method is based on atom probe tomography (APT), a spatially resolved mass spectrometry technique, which can map atomic positions in 3D and reveal the chemical identity of the constituent atoms in the protein. This method could open up new possibilities to study biological structures[4] and their interactions with near atomic resolution.

Dr. G. Sundell, Dr. M. Hulander, A. Pihl, Prof. M. Andersson
Department of Chemistry and Chemical Engineering
Chalmers University of Technology
Gothenburg 41296, Sweden
E-mail: martin.andersson@chalmers.se

The ORCID identification number(s) for the author(s) of this article can be found under https://doi.org/10.1002/smll.201900316.

DOI: 10.1002/smll.201900316

The 3D structure of a protein is intrinsically linked to its chemical properties,[5] which ultimately determines its physiological role. Therefore, knowledge of the 3D structure is often key for understanding fundamental biochemical processes, e.g., the catalytic mechanism of an enzyme or how a drug interacts with its biological target.[6]

Over the years, the structural biologist's primary tool for structural investigation of proteins and other biomolecules has been X-ray crystallography. This method requires purification and growth of protein crystals that scatter X-rays in a periodic manner. Smaller protein structures and protein fragments can be solved using NMR spectroscopy. In recent years, the development of direct electron detectors and tomographic techniques has enabled a revolution in cryo-electron microscopy for use in structural biology.[3,7] As a consequence, a remarkable number of complex protein structures have been solved and made available to the scientific community via online databases.[8,9] Although the methods for structural analysis of biomolecules outlined above in many ways complement each other, gaps in utility still exist. As the complexity of the studied systems increase, there is a need to further expand the analytical toolbox in structural biology.

Herein, we demonstrate an entirely new method for structural analysis of proteins and biomolecules based on APT. APT is a rapidly developing technique in the field of materials analysis, which in the last decade has progressed from being used almost exclusively for analysis of metals and alloys, to now routinely perform atomic scale investigations of semiconductors,[10] geological materials,[11] and biominerals.[12]

The fundamental principle of this technique is based on ejection—field evaporation—of individual ions or molecules from a needle-shaped specimen (radius < 100 nm) by the application of a strong electric field (>1 V Å^{-1}) and illumination with short laser pulses.[13] The impact position of each field evaporated ion on a position-sensitive detector is recorded providing lateral (*X*–*Y*) resolution. The sequence of ions that hit the detector gives the depth (*Z*) coordinate. The flight-time of ions reveals the mass-to-charge-state ratio. With these data, a 3D reconstruction of the sample can be assembled, wherein the chemical identity of each ionic species usually can be deduced. A schematic overview of the technique is presented

in **Figure 1**a. One limitation of APT is that the strong electric field around the needle induces large mechanical stresses in the sample, so-called Maxwell stresses.[14] As a result, an atom probe experiment typically ends with a mechanical fracture of the specimen. Specimen fracture and field-induced deformation has therefore, to date, largely precluded routine atom probe analysis of soft materials.[15] Notable exceptions include studies of ferritin clusters[16] and molecules,[17,18] mammalian and bacterial cells,[19,20] and organic fibers in the chiton tooth.[21]

In the present work, we used a sol–gel method to embed rabbit immunoglobulin G (IgG)[22] in a solid silica matrix. This method of biomolecule entrapment can be performed at room temperature and has previously been shown to preserve proteins in their native and functional state.[23] The resulting glassy silica (depicted in Figure 1b) allows for a subsequent focused ion beam-scanning electron microscope (FIB-SEM) in situ lift-out procedure, followed by a tip-sharpening step commonly employed for atom probe specimen preparation.[24,25] The final specimen tip is depicted in the SEM micrograph in Figure 1c, and the entire process is overviewed in Figure S4 in the Supporting Information. Crucially, the silica matrix also provides the needle-shaped specimen with sufficient mechanical integrity to permit atom probe analysis. The solid glass structure does not deform significantly or rupture prematurely in the presence of the strong electric field, which allows for field evaporation of surface atoms as ions in a controlled manner. Thereby, we could perform direct APT analysis of a single protein, without the need for significant modifications of existing APT data reconstruction protocols.

We prepared amorphous solid silica using the alkoxide tetraethyl orthosilicate (TEOS) or sodium silicate (water glass) as silica precursor to evaluate two different embedding procedures. Silicon alkoxides spontaneously hydrolyze upon contact with water and condensate to form an inorganic, amorphous, polymer network of silicon and oxygen, leaving an alcohol as the by-product. The reaction is catalyzed both by acidic and basic conditions and is foremost dependent on the organic moieties of the alkoxide, pH, concentration, and temperature. By varying these parameters, the gelling time and physical properties (e.g., porosity) of the formed solid can be controlled.[26]

Successful silica synthesis for protein analysis using APT relies on a compromise between maintaining a suitable chemical environment for the protein of interest, while still forming a sufficiently strong silica matrix. We note that different synthesis conditions may be necessary depending on the protein in question, to avoid denaturation or aggregation. For example, silica glasses derived from TEOS at neutral pH resulted in a porous silica matrix with too low mechanical stability for APT. Acidic conditions, on the other hand, rendered a high-density silica matrix that could readily withstand the mechanical stresses during the APT analysis. (Data from porosity measurements using Brunauer–Emmett–Teller (BET) are available in Section S1, Supporting Information.) As seen in the fluorescence microscopy image, Figure 1d, where fluorescein isothiocyanate (FITC)-conjugated IgG was embedded in silica synthesized from TEOS at low pH, large protein aggregates were clearly visible in the sample. IgG is generally prone to aggregation, and the F_c region of the protein is particularly susceptible to aggregation in acidic environments.[27] Remarkably,

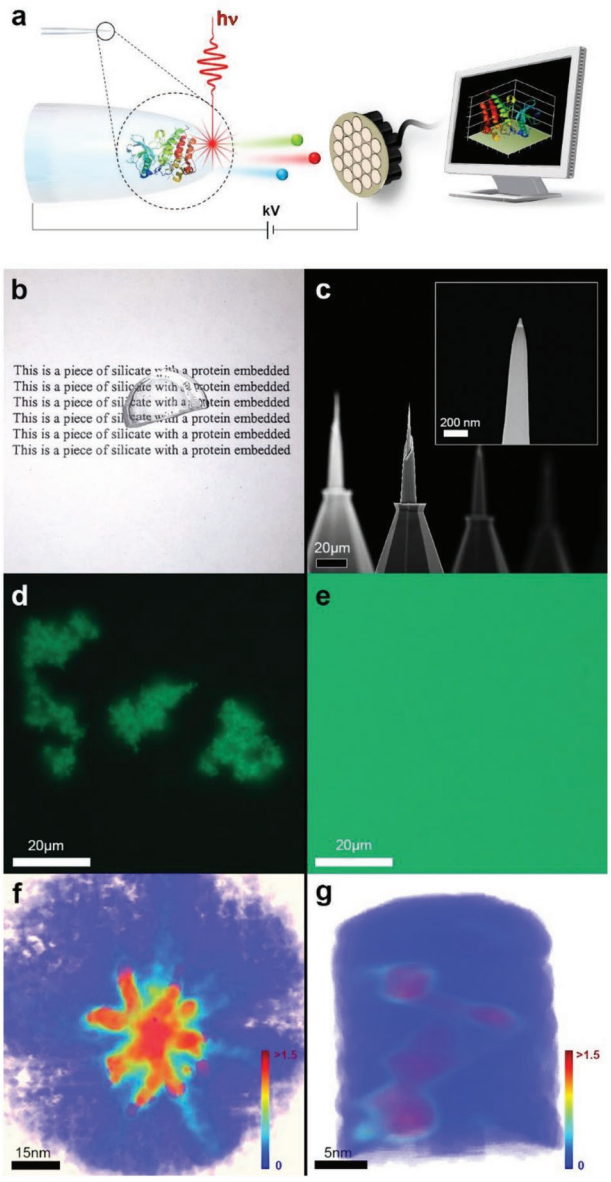

Figure 1. Overview of the described method and influence of the embedding matrix on protein stability. a) Schematic overview of the procedure for single protein analysis using APT; after embedding of the protein into a silica matrix the sample is sharpened to an ultra-fine tip (radius < 100 nm). The tip is then subjected to a high electric field under illumination with a pulsed laser to induce field evaporation of the surface ions. The data from a position-sensitive time-of-flight mass spectrometry detector are compiled into a 3D reconstruction of the original sample with near-atomic resolution. b) Macro photograph of a bulk piece of the synthesized protein-containing silica matrix. c) SEM micrograph (600X magnification) of an array of protein-containing specimen tips sharpened using FIB. Insert: SEM micrograph of individual specimen apex at 100 000X magnification. d,e) Fluorescence microscopy images acquired through a 100X objective of FITC-labeled IgG embedded in the two different silica matrices. Large aggregates are c) clearly visible when the matrix is prepared from TEOS at pH 2, but d) indiscernible in the water glass–based synthesis at pH 7. f) A pentameric aggregate of IgG is visible in a 2D heatmap (atomic number density of organic species) from an atom probe analysis with TEOS-derived silica at pH 2 as the embedding matrix. g) Heatmap (atomic number density of organic species) of a single molecule of IgG embedded in a silica matrix using a water glass–based synthesis at pH 7.

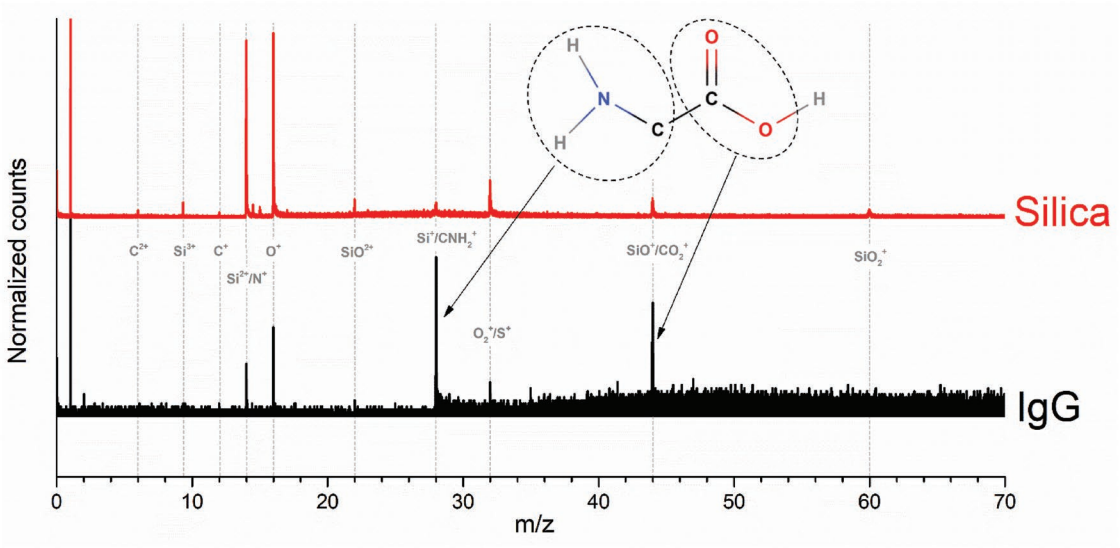

Figure 2. Atom probe mass spectra. Annotated mass spectra in linear scale from the water glass–derived silica matrix (red) and the IgG subvolume (black) of an atom probe analysis. The peaks from amino acid trace ions are indicated with arrows.

atom probe analysis of these samples not only confirmed IgG aggregation, but also provided details about the aggregates; the APT reconstruction in Figure 1f appears to show a pentameric aggregate, where the variable F_{ab} domains are pointing outward, with the F_c regions centrally conjoined. Similar complexes formed by interactions between F_c domains have been observed to trigger complement activation.[28]

The simplest form of aqueous silica is orthosilicic acid ($Si(OH)_4$) and is readily available in the form of commercial sodium silicate solutions (water glass). At concentrations above $\approx 1 \times 10^{-3}$ M auto-polycondensation occurs at room temperature and monomers start to polymerize into nanosized aggregates, that eventually form the solid amorphous silica matrix as water evaporates.[29] Since aqueous sodium silicate solutions are inherently basic, we adjusted pH to physiological values by using an acidic ion exchange column before adding the protein. By using this approach, no protein aggregates of FITC-IgG were observed in the silica matrix at the magnification provided by fluorescence microscopy (Figure 1e). Electron transparent foils of the silica matrix were prepared using FIB-SEM, and bright field transmission electron microscopy (TEM) confirmed that monomers with the characteristic "Y-shaped" structure of IgG were encapsulated inside the silica matrix (Figure 3a). However, at this resolution we are not provided any details about possible changes in secondary structure or rearrangements of amino acid side chains as a result of the sol–gel process.

The mechanical strength of water glass–derived silica allowed for controlled atom probe analysis without premature specimen fracture. To assemble the acquired data into tomograms, we used a standard voltage evolution–based reconstruction protocol for APT.[30] As the water glass precursor is inorganic, we could use the carbon-containing ionic species in the reconstruction to unambiguously map out IgG in the silica matrix (see Figure 1g). Due to the strong electric fields and the fundamentally different ionization process, the APT mass spectra from IgG (see **Figure 2**) differ significantly from those obtained with other mass spectrometry techniques.[31] Dominant organic ions are the amino acid traces CNH_2^+—likely originating mostly from a combined amine group-α-carbon ion—and CO_2^+—likely mostly from the carboxyl functional group. At present, we are not able to identify individual amino acid side chains in the spectra. CON^+ and $C_2O_2^+$ (or possibly NH_2-C-CO^+) at 42 and 56 Da, respectively, were also present in the pentameric aggregate (Figure S2, Supplementary Information). Mass spectra of the glass and the protein share some common peaks. Thus, the N^+ peak at 14 Da is indistinguishable from the ubiquitous Si^{2+} signal, which makes identification of individual nitrogen atoms difficult. Sulfur atoms, which participate in the intra amino acid chain disulfide bonding, are not discernible due to an overlap with the more abundant O_2^+ ions that originate from the silica structure. At present, isotopic labeling is required to distinguish these species. (For mass spectra of the TEOS derived silica, please see Section S2, Supporting Information.)

As a result of the overlapping peaks, quantification of atomic species could only reliably be performed for carbon. The detection efficiency of the atom probe instrument in this study is stated by the manufacturer to be 37%. After a background subtraction and natural isotopic abundancy decomposition, a total number of 2370 carbon atoms were detected. Accounting for the detection efficiency of the instrument, this gives 6405 carbon atoms, which is in good agreement with the number of carbon atoms that have been reported for rabbit IgG isomers in the literature.[22] It is also noteworthy that the major characteristic peaks of water at 17, 18, and 19 Da[32] were absent in the analyses of IgG, which suggest that the hydration shell around the molecule was completely replaced with silica during the condensation process. However, oxygen and hydrogen peaks are omnipresent throughout the analysis, and presence of water cannot be ruled out.

The spatial distribution of each carbon-containing ionic species of the molecule is presented in **Figure 3**b. 3D heat maps

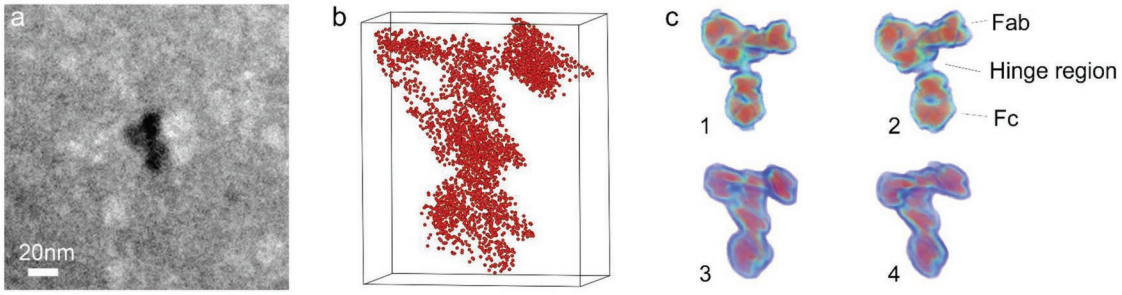

Figure 3. TEM micrograph and atom probe 3D reconstructions. a) Bright field TEM micrograph of a single IgG molecule embedded in a water glass–derived silica matrix. b) Spatial distribution of organic ionic species (CNH_2^+ and CO_2^+) in an IgG subvolume of an APT reconstruction from the water glass with embedded IgG, retrieved by generating an isodensity region with the filtering criterion > 6 C atoms nm^{-3}. c1,2) carbon isodensity heat map (5 C atoms nm^{-3}) of human IgG as reported by Saphire et al.[5] and regenerated in the atom probe 3D visualization software and 3,4) the equivalent isodensity surface from our APT analysis, retrieved from the isodensity region in (c).

of the atomic number density can also be used to illustrate the structure of the protein (Figure 3c). The spatial resolution in APT is anisotropic, and typically better along the direction of analysis than laterally.[33] Therefore, it is difficult to estimate an exact global value for the reconstruction. However, the F_{ab} loop is clearly visible, which could indicate a resolution of at least 15 Å.

Due to the inherent flexibility of hinge regions, crystallographic structural data for antibodies in their entirety are scarce. To the best of our knowledge, the only reported complete rabbit IgG structure is the result of small angle scattering experiments.[22] In this study, previously solved crystallized F_{ab} and F_c fragments and hinge region models were fitted with the scattering data. Instead, we used the structure of human IgG, determined by X-ray diffraction at 2.7 Å resolution, as a reference (Protein Data Bank entry 1HZH).[5] By importing the reported structure data into the atom probe data analysis software, direct visual comparison with our APT reconstruction could be made (see Figure 3c). We note again that the detector efficiency of the atom probe used in this study was 37%, whereas the reference structure includes all atoms in the protein except hydrogens. Despite this fact, the APT atomic number density map is still in good agreement with the reference structure.[5]

In summary, we herein report a fundamentally new method for protein analysis on the subnanometer scale using APT. With further development, this technique may be capable of concurrently providing 3D structural information and reveal the chemical identity of constituent atoms in an individual protein. The resolution of an atom probe experiment can, in ideal cases, approach 1 Å.[33] While it is probably unrealistic to expect similar performance for the analysis of biomolecules, we believe that information can be gained at least on the level of protein tertiary structure. Moreover, the fact that single molecules are analyzed individually means that variable conformations of flexible proteins could potentially be captured.

At present, we cannot ascertain that the protein retains its exact functional structure after the sol–gel process. As the water is exchanged for silica, it is reasonable to expect at least minor conformational changes in response,[34] for instance rearrangements of hydrophilic amino acid side chains. However, silica-encapsulated enzymes can reportedly retain their catalytic activity[35] and even remain entirely unperturbed, as evident from solid-state NMR studies.[23]

We acknowledge that the porous nature of the silica structure introduces some uncertainties with regards to the reconstruction protocol, and poses risk of premature specimen failure. Somewhat surprisingly, nanoporous materials can, in many cases, be analyzed with reasonable accuracy using APT.[36,37] We would intuitively expect differences in evaporation field between the protein and the surrounding silica matrix. This can lead to distortions in the 3D reconstruction.[38] However, large differences in evaporation field typically result in sharp voltage drops as the low-field phase evaporates. No major voltage drops occurred across the transition from silica matrix to protein, and back to matrix. A possible explanation for this could be penetration and intercalation of silica into the protein interior, resulting in an elevated evaporation field, close to that of the matrix. Most organic ions appear as molecular CNH_2^+ and CO_2^+ peaks in our spectra. Such ions stemming from organic fibers have been observed in prior investigations of dentin,[12] enamel,[39] and bone,[37,40] and are seemingly characteristic of APT mass spectra from biomolecules in hard matrices.

Given that the probed volume in APT is extremely small, protein concentration in the silica should ideally be such that any given analysis volume from the matrix (typically smaller than 10^5 nm^3) contains at least one molecule of interest. Further work on sol–gel glass synthesis will be required to routinely produce such glasses. The standard FIB-SEM-based sample preparation protocol for APT requires no more than approximately 50 fL of material to produce three to four needle-shaped specimens. In our experiments, we typically obtained data volumes in the range of 10^6–10^7 ions per analysis from the water glass before specimen fracture. If the molecules of interest can be evenly dispersed in the silica matrix, protein quantities as small as 10^{-16} moles could in theory be sufficient for structural analysis with APT. This could make the technique useful in tandem with lab-on-a-chip type experimental platforms,[41] where minute volumes of liquids are studied.

Finally, we note that commercial state-of-the-art APT detectors are capable of detection efficiencies in excess of 80%. There are realistic prospects for development of new ion detection concepts that can be applied in APT in the near future.[42,43] If these ideas come to fruition, one single atom probe analysis with 100% detection efficiency and ionic kinetic energy discrimination could reveal each atomic position in a

single protein, without the chemical ambiguity that arises from spectral overlaps. This could significantly further our understanding of complex biomolecular systems, such as interactions between ligands and cell receptors or metal ion chelation in heme centers of proteins. Such advances could spark a revolution in atom probe for nano biology applications similar to that recently instigated by direct electron detectors in cryo-electron microscopy.

Experimental Section

Protein Encapsulation using TEOS pH 2: All chemicals were purchased from Sigma-Aldrich and used without further purification. Water used in experiments was deionized and filtered through a Milli-Q system, Millipore, and all prepared solutions were sterile filtered before use. Experimental design was adopted and modified from Chang and Ring[44] In a typical experiment, 1 mL TEOS (reagent grade, 98% pure), 2.1 mL EtOH (95% pure), and 90 µL HCl (12 M) was added to a sample flask, in an ice bath, and vigorously stirred for 10 min. To the mixture 990 µL water and 200 µL IgG (10 mg mL^{-1}) was added under continuous stirring. The protein-containing silicate solution was then left to cure at 37 °C for minimum 24 h.

Protein Encapsulation using TEOS pH 7: All chemicals were purchased from Sigma-Aldrich and used without further purification. Water used in experiments was deionized and filtered through a Milli-Q system, Millipore, and all prepared solutions were sterile filtered before use. Experimental procedure was adopted and modified from Ferrer et al.[45] In a typical experiment, 2 mL TEOS (reagent grade, 98% pure), 972 µL water, and 61 µL HCl (0.1 M) was added to a sample flask which was sealed with lid and parafilm. The mixture was sonicated (USC 900 THD; VWR International) at 45 kHz at 600 W for 60 min. Prompt gelling was avoided by addition of 4 mL water.

The ethanol formed during hydrolysis was removed by rotary evaporation (Buchi Rotavapor system) at 40 °C and approximately 90 mbar for 20 min. The weight of the sample was noted before and after rotary evaporation. 0.7376 g (ρ = 1.22 g mL^{-1}) of the sample was transferred to a new flask, and to avoid instant gelling the sample was kept on wet ice. 6.6 µL Sörensens's phosphate buffer (0.1 M, pH 7.4) and 50 µL IgG (10 mg mL^{-1}) was then added. The sample was vortexed for a few seconds and left to cure at 37 °C for minimum 24 h.

Protein Encapsulation using Water Glass: All chemicals were purchased from Sigma-Aldrich and used without further purification (except polyclonal rabbit anti-human C3c Complement/FITC that was purchased from Dako Cytomation). Water used in experiments was deionized and filtered through a Milli-Q system, Millipore, and all prepared solutions were sterile filtered before use. A method developed from Bhatia et al.[46] was used. To adjust the pH to physiological values, an acidic ion exchange column was prepared by placing glass wool at the bottom of a plastic syringe and subsequent placing 1 g of ion-exchange resin (Dowex 50WX8 hydrogen form 50–100 mesh) on top. Activation of the ion-exchange resin was made by washing with 3 mL of NaOH (4 M), 12 mL of EtOH (95% pure), and 10 mL of water. The activation was continued by rinsing with 3 mL HCl (3 wt%) followed by rinsing with Milli-Q water until the eluate reached neutral pH. Neutral silicate solution was achieved by allowing 1 mL sodium silicate solution (1:1 weight ratio of water and sodium silicate with 28.7 wt% SiO_2, 8.9 wt% Na_2O) eluate through the column into a sample flask. 100 µL of the prepared silicate solution was transferred to a sample vial and 47 µL polyclonal rabbit anti-human C3c Complement/FITC (3.8 mg mL^{-1} with an FITC/protein ratio of 2.5) was added. The protein-containing silicate solution was vortexed for a few seconds and applied as small droplets (10 µL) onto microscope glass slides and left to cure at 37 °C (≥48 h).

Physisorption Measurement: The porosity of the formed silica was investigated with nitrogen physisorption measurement. The samples were prepared using the described methods with the exception that no proteins were added. Samples were ground to a fine powder using a mortar, and degassed in vacuum oven (1 h 75 °C followed by 4 h incubation at 125 °C) prior to measurement on a TriStar 3000 instrument.

Fluorescence Microscopy: Images were captured using an Axio Imager Z2m microscope (Carl Zeiss GmbH), equipped with an HBO 100 light source and an Axiocam 506 camera, using the filter GFP, 38HE ($\lambda_{Excitation}$: 470 nm and $\lambda_{Emission}$: 525 nm).

Preparation of Samples for Electron Microscopy: Samples were attached to aluminium SEM sample holders with adhesive carbon tape and sputtered with a 20 nm Pd layer to enhance conductivity, protect the surface from damage from ion and electron beams, and minimize charging in the microscope.

TEM Sample Preparation and Imaging: Electron transparent thin foils from the glass was prepared according to established protocols[47] using a combined focused ion beam and SEM workstation (FEI Versa 3D, FEI Company, The Netherlands). Over the region of interest, a 3 × 12 µm Pt strip of 2 µm thickness was deposited using ion (Ga^+) beam deposition (50 pA, 30 kV). Pt deposition occurred by scanning the ion beam over the area of interest, so that secondary electrons interacted with and decomposed an organometallic precursor gas ($(C_5H_4)CH_3Pt(CH_3)_3$) that was injected into the chamber. Two trenches were subsequently milled out (5 nA, 30 kV) on both sides of the Pt strip. The sample was then tilted and the foil was milled loose on three sides (3 nA, 30 kV). A sharp (radius < 2 µm) tungsten micromanipulator needle (Omniprobe) was inserted into the chamber and attached to the sample foil. The remaining side connecting the foil with the substrate was milled off. The foil was attached to a copper TEM half-grid by means of Pt deposition. The foil was then thinned to a thickness of less than 100 nm, using decreasing ion currents and acceleration voltages (from 0.5 nA, 30 kV down to 7.7 pA, 5 kV). TEM was performed on an FEI Tecnai T20 instrument (FEI Company, Eindhoven, The Netherlands), equipped with a LaB_6 electron emitter. The images were acquired in bright field mode with a CCD camera at slight underfocus to enhance contrast and the microscope was operated at 200 kV acceleration voltage.

APT Sample Preparation: Atom probe samples were prepared using a standard in situ liftout procedure with a focused ion beam SEM (FEI Versa 3D). A 2 × 20 µm Pt strip was deposited over the region of interest (50 pA, 30 kV). Trenches were milled underneath the Pt strip at an angle of 30° to surface normal (5 nA, 30 kV). Thus, a wedge was formed underneath the Pt strip. The wedge was cut free on one side and a micromanipulator needle (Omniprobe) was inserted and attached to the wedge by means of Pt deposition (50 pA, 30 kV). The other side of the wedge was released from its connection to the substrate (0.5 nA, 30 kV). 2 µm segments of the wedge were then attached to the top of Si microtip posts (Cameca Scientific Instruments) by Pt deposition. Sharp tips (radii < 50 nm) were milled out from the wedge segments by annual ion milling patterns (from 0.5 nA, 30 kV to 7,7 pA, 5 kV), where the radii of the pattern were made smaller and smaller.

APT Methods: APT analysis was performed using a local electrode atom probe (Imago LEAP 3000 X HR). Samples were analyzed in laser-pulsed mode using a green laser (λ = 532 nm) at pulse frequencies 100–200 kHz and pulse energies 0.25–0.5 nJ. The average evaporation rate during analysis was maintained between 0.0025 and 0.005 ions per pulse. The base temperature of the tip was kept at 30 or 50 K and the pressure in the chamber was held below 10^{-8} Pa.

Atom probe reconstructions were performed using the Cameca Integrated Visualization and Analysis Software (IVAS), versions 3.4.3 and 3.6.6. Typically the reconstructions were performed based on the voltage evolution during analysis.[48] The field factor k_f was set 5. The evaporation field of the silica was measured to be approximately 27 V $Å^{-1}$, based on SEM examinations of tip radius before and after analysis. The average volume ascribed to each atom in the reconstructions was set to 0.02 nm^3.

Atomic number density heat maps were created by dividing the analysis volume into a voxel grid of 0.2 × 0.2 × 0.2 nm^3, using delocalization parameters 1.0 nm in *x* and *y* and 0.5 in *z*.

The reference protein data bank IgG structure was retrieved from the PDB ID 4GDQ.[49] The data imported into IVAS by taking the positional atomic coordinates from the .PDB file and generating a .POS file. The

rabbit IgG molecule was analyzed using the UCSF Chimera software version 1.11.2.[50]

Supporting Information

Supporting Information is available from the Wiley Online Library or from the author.

Acknowledgements

M.A. and M.H. formed the initial concept. M.A. directed the research. G.S. performed the APT measurements and TEM imaging. M.H. and A.P. developed the silica embedding procedure. M.H. performed the SEM imaging and artwork. A.P. performed the BET measurements and FL imaging. All authors wrote the manuscript. First and second authors contributed equally to the paper and hence their order was determined by the stochastic "rock, paper, scissors" method. The Wallenberg foundation, through their KAW fellow program (MA), and Chalmers Area of Advance-Material Science are acknowledged for financial support.

Conflict of Interest

The authors declare no conflict of interest.

Keywords

atom probe tomography, immunoglobulin G, mass spectrometry, structural biology, sol–gel

Received: January 18, 2019
Revised: April 1, 2019
Published online: May 6, 2019

[1] H. N. Chapman, P. Fromme, A. Barty, T. A. White, R. A. Kirian, A. Aquila, M. S. Hunter, J. Schulz, D. P. DePonte, U. Weierstall, *Nature* **2011**, *470*, 73.
[2] K. Wuthrich, *Science* **1989**, *243*, 45.
[3] E. Callaway, *Nature* **2015**, *525*, 172.
[4] D. Avnir, S. Braun, O. Lev, M. Ottolenghi, *Chem. Mater.* **1994**, *6*, 1605.
[5] E. O. Saphire, P. W. H. I. Parren, R. Pantophlet, M. B. Zwick, G. M. Morris, P. M. Rudd, R. A. Dwek, R. L. Stanfield, D. R. Burton, I. A. Wilson, *Science* **2001**, *293*, 1155.
[6] V. Lounnas, T. Ritschel, J. Kelder, R. McGuire, R. P. Bywater, N. Foloppe, *Comput. Struct. Biotechnol. J.* **2013**, *5*, 1.
[7] W. Kühlbrandt, *Science* **2014**, *343*, 1443.
[8] H. M. Berman, J. Westbrook, Z. Feng, G. Gilliland, T. N. Bhat, H. Weissig, I. N. Shindyalov, P. E. Bourne, *Nucleic Acids Res.* **2000**, *28*, 235.
[9] C. L. Lawson, M. L. Baker, C. Best, C. Bi, M. Dougherty, P. Feng, G. van Ginkel, B. Devkota, I. Lagerstedt, S. J. Ludtke, R. H. Newman, T. J. Oldfield, I. Rees, G. Sahni, R. Sala, S. Velankar, J. Warren, J. D. Westbrook, K. Henrick, G. J. Kleywegt, H. M. Berman, W. Chiu, *Nucleic Acids Res.* **2011**, *39*, D456.
[10] T. F. Kelly, D. J. Larson, K. Thompson, R. L. Alvis, J. H. Bunton, J. D. Olson, B. P. Gorman, *Annu. Rev. Mater. Res.* **2007**, *37*, 681.
[11] J. W. Valley, A. J. Cavosie, T. Ushikubo, D. A. Reinhard, D. F. Lawrence, D. J. Larson, P. H. Clifton, T. F. Kelly, S. A. Wilde, D. E. Moser, *Nat. Geosci.* **2014**, *7*, 219.
[12] L. M. Gordon, L. Tran, D. Joester, *ACS Nano* **2012**, *6*, 10667.
[13] M. K. Miller, A. Cerezo, M. G. Hetherington, G. D. W. Smith, *Atom Probe Field Ion Microscopy*, Oxford Science Publications, Clarendon Press, Oxford **1996**.
[14] M. K. Miller, R. G. Forbes, *Atom-Probe Tomography: The Local Electrode Atom Probe*, Springer Science+Business Media, New York **2014**.
[15] T. F. Kelly, O. Nishikawa, J. A. Panitz, T. J. Prosa, *MRS Bull.* **2009**, *34*, 744.
[16] J. A. Panitz, *Ultramicroscopy* **1982**, *7*, 241.
[17] J. A. Panitz, D. C. Ghiglia, *J. Microsc.* **1982**, *127*, 259.
[18] D. E. Perea, J. Liu, J. Bartrand, Q. Dicken, S. T. Thevuthasan, N. D. Browning, J. E. Evans, *Sci. Rep.* **2016**, *6*, 22321.
[19] K. Narayan, T. J. Prosa, J. Fu, T. F. Kelly, S. J. Subramaniam, *J. Struct. Biol.* **2012**, *178*, 98.
[20] V. R. Adineh, R. K. W. Marceau, T. Velkov, J. Li, J. Fu, *Nano Lett.* **2016**, *16*, 7113.
[21] L. M. Gordon, D. Joester, *Nature* **2011**, *469*, 194.
[22] L. E. Rayner, N. Kadkhodayi-Kholghi, R. K. Heenan, J. Gor, P. A. Dalby, S. J. Perkins, *J. Mol. Biol.* **2013**, *425*, 506.
[23] M. Fragai, C. Luchinat, T. Martelli, E. Ravera, I. Sagi, I. Solomonov, Y. Udi, *Chem. Commun.* **2014**, *50*, 421.
[24] K. Thompson, D. Lawrence, D. J. Larson, J. D. Olson, T. F. Kelly, B. Gorman, *Ultramicroscopy* **2007**, *107*, 131.
[25] M. K. Miller, K. F. Russell, G. B. Thompson, *Ultramicroscopy* **2005**, *102*, 287.
[26] C. J. Brinker, *J. Non-Cryst. Solids* **1988**, *100*, 31.
[27] A. W. P. Vermeer, W. Norde, *Biophys. J.* **2000**, *78*, 394.
[28] C. A. Diebolder, F. J. Beurskens, R. N. de Jong, R. I. Koning, K. Strumane, M. A. Lindorfer, M. Voorhorst, D. Ugurlar, S. Rosati, A. J. R. Heck, J. G. J. van de Winkel, I. A. Wilson, A. J. Koster, R. P. Taylor, E. O. Saphire, D. R. Burton, J. Schuurman, P. Gros, P. W. H. I. Parren, *Science* **2014**, *343*, 1260.
[29] D. J. Belton, O. Deschaume, C. C. Perry, *FEBS J.* **2012**, *279*, 1710.
[30] D. J. Larson, T. Prosa, R. Ulfig, B. Geiser, T. Kelly, *Local Electrode Atom Probe Tomography: A User's Guide*, Springer Science+Business Media, New York **2013**, p. 109.
[31] Z. Zhang, H. Pan, X. Chen, *Mass Spectrom. Rev.* **2009**, *28*, 147.
[32] D. K. Schreiber, D. E. Perea, J. V. Ryan, J. E. Evans, J. D. Vienna, *Ultramicroscopy* **2018**, *194*, 89.
[33] B. Gault, M. P. Moody, F. de Geuser, D. Haley, L. T. Stephenson, S. P. Ringer, *Appl. Phys. Lett.* **2009**, *95*, 034103.
[34] Y. Geiger, H. E. Gottlieb, Ü. Akbey, H. Oschkinat, G. Goobes, *J. Am. Chem. Soc.* **2016**, *138*, 5561.
[35] R. Obert, B. C. Dave, *J. Am. Chem. Soc.* **1999**, *121*, 12192.
[36] M. K. Miller, L. Longstreth-Spoor, K. F. Kelton, *Ultramicroscopy* **2011**, *111*, 469.
[37] B. Langelier, X. Wang, K. Grandfield, *Sci. Rep.* **2017**, *7*, 39958.
[38] M. K. Miller, M. G. Hetherington, *Surf. Sci.* **1991**, *246*, 442.
[39] L. M. Gordon, D. Joester, *Front. Physiol.* **2014**, *5*, 509.
[40] G. Sundell, C. Dahlin, M. Andersson, M. Thuvander, *Acta Biomater.* **2017**, *48*, 445.
[41] C. Hansen, S. R. Quake, *Curr. Opin. Struct. Biol.* **2003**, *13*, 538.
[42] T. F. Kelly, *Microsc. Microanal.* **2011**, *17*, 1.
[43] T. F. Kelly, M. K. Miller, K. Rajan, S. P. Ringer, *Microsc. Microanal.* **2013**, *19*, 652.
[44] S. Y. Chang, T. A. Ring, *J. Non-Cryst. Solids* **1992**, *147–148*, 56.
[45] M. L. Ferrer, F. Del Monte, D. Levy, *Chem. Mater.* **2002**, *14*, 3619.
[46] R. B. Bhatia, C. J. Brinker, A. K. Gupta, A. K. Singh, *Chem. Mater.* **2000**, *12*, 2434.
[47] L. A. Giannuzzi, F. A. Stevie, *Micron* **1999**, *30*, 197.
[48] P. Bas, A. Bostel, B. Deconihout, D. Blavette, *Appl. Surf. Sci.* **1995**, *87–88*, 298.
[49] L. E. Rayner, N. Kadkhodayi-Kholghi, R. K. Heenan, J. Gor, P. A. Dalby, S. J. Perkins, *J. Mol. Biol.* **2013**, *425*, 506.
[50] E. F. Pettersen, T. D. Goddard, C. C. Huang, G. S. Couch, D. M. Greenblatt, E. C. Meng, T. E. Ferrin, *J. Comput. Chem.* **2004**, *25*, 1605.

